Eur. Phys. J. A **9**, 537–552 (2000)

THE EUROPEAN PHYSICAL JOURNAL A

Pion absorption reactions on N, Ar and Xe

B. Kotliński[7,a], D. Androić[8], G. Backenstoss[1], D. Bosnar[8], H. Döbbeling[7], T. Dooling[6], M. Furić[8], P.A.M. Gram[3], N.K. Gregory[4], A. Hoffart[2,7], C.H.Q. Ingram[7], A. Klein[6], K. Koch[7], J. Köhler[1], M. Kroedel[1], G. Kyle[5], A. Lehmann[1,7], V. Markushin[7], A.O. Mateos[4], K. Michaelian[7], T. Petković[8], M. Planinić[8], R.P. Redwine[4], D. Rowntree[4], N. Šimičević[4], R. Trezeciak[2], H.J. Weyer[1,7], M. Wildi[1], and K.E. Wilson[4]
The LADS Collaboration

[1] University of Basel, CH-4056 Basel, Switzerland
[2] University of Karlsruhe, D-76128 Karlsruhe, Germany
[3] LAMPF, Los Alamos NM 87545, USA
[4] Massachusetts Institute of Technology, Cambridge MA 02139, USA
[5] New Mexico State University, Las Cruces NM 88003, USA
[6] Old Dominion University, Norfolk VA 23529, USA
[7] Paul Scherrer Institute, CH-5232 Villigen PSI, Switzerland
[8] University of Zagreb, HR-10000 Zagreb, Croatia

Received: 16 October 2000
Communicated by M. Garçon

Abstract. The absorption of π^+ on Ar was studied at pion energies of 70, 118, 162, 239 and 330 MeV, and on N and Xe at 239 MeV. Twenty-six absorption reaction channels with at least two energetic charged particles in the final state have been evaluated. Partial cross-sections have been determined according to the number of protons, neutrons and deuterons in the final state.

PACS. 25.80.Ls Pion inclusive scattering and absorption

1 Introduction

The primary process for pion absorption on heavy nuclei ($A > 10$) is thought to be the absorption on two nucleons (2NA), usually an $I = 0$ pn pair. However, several past experiments have shown that the 2NA cross-section does not exhaust the total absorption cross-section [1–3]. Pion absorption with the emission of more than two energetic nucleons (multi-nucleon absorption) was observed in experiments [4–7] detecting at least three protons in the final state (3p). From these data, it is known that the strength of multi-nucleon absorption across the Δ-resonance region is significant. Though we have a broad knowledge of its strength, the detailed origin of multi-nucleon absorption is still not clear [8,9].

To gain insight into the origins of multi-nucleon absorption, some questions need to be resolved experimentally. For example, the contributions from final states with neutral particles need to be established, *e.g.*, how does the 3p cross-section compare to that for two protons and a neutron (2p1n)? What is the strength of the final states with more than three energetic particles, *e.g.*, four protons (4p)? What is the importance of deuterons in the final state? And what are the energy and target mass dependences for each final state? The work presented in this paper addresses these issues.

Some attempts to answer these questions have been made in previous experiments. Bauer *et al.* [6] estimated the four nucleon (4N) cross-section on an oxygen target based on their measured 3p distributions. The experiment did not analyse neutral particles and had poor angular resolution. Tacik *et al.* [10] also directly measured 3p events on a carbon target and from that estimated the 4N cross-section. Again this experiment was insensitive to neutral particles and suffered from limited solid angle coverage. In ref. [11] estimates of 4N and 3N cross-sections on a carbon target were made, but they were inferred from the measurement of the 2p distributions.

The most complete pion multi-nucleon measurement on heavy targets until now have been made by the "BGO-ball" experiments at LAMPF in which 3p and 2p events were measured over a wide range of targets (lithium to lead) and a wide range of pion energies (50–500 MeV) [7, 12,13]. Deuterons were also measured in 1p1d and 2p1d events. The experiment had nearly 4π solid angle and detected neutral particles. However, it did not have good neutral particle identification, and therefore reliable separation between neutrons and photons was not possible.

All past experiments suffered from limitations either in phase space coverage, kinematic definition, particle identi-

[a] e-mail: bohdan.kotlinski@psi.ch

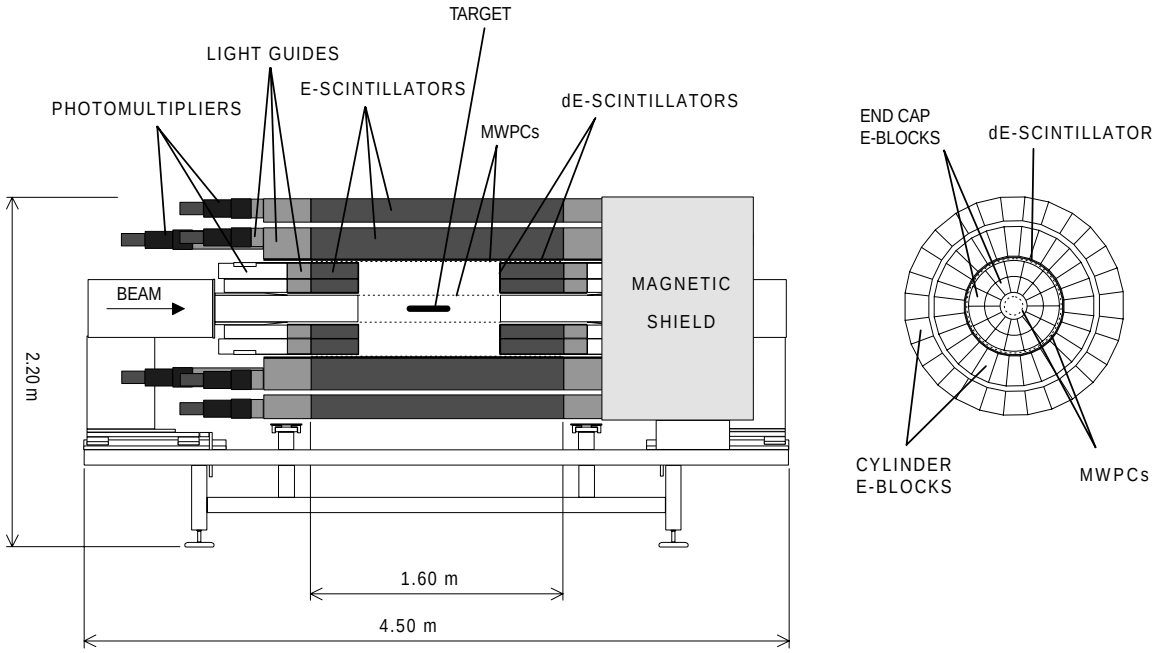

Fig. 1. Side view and end view of the LADS detector.

fication, or statistical accuracy for the multi-nucleon channels. In none of the above experiments events with four energetic particles were directly measured (here we consider 2p1d as a three-particle state).

In the present paper we report results for the multi-nucleon π^+ absorption reaction on N, Ar and Xe at various pion energies. The N and Xe data are presented for a single incident pion energy of 239 MeV, and the Ar data for five pion energies 70, 118, 162, 239 and 330 MeV. In addition Xe data at 118 and 162 MeV have been analyzed in a similar way in ref. [14]. The data analyzed in this paper have some overlap with a previous LADS analysis [15] which was optimized to determine the total pion absorption cross-section reliably. Evidence for the existence of Initial State Interaction (ISI) in pion absorption on N, Ar and Xe has been reported by our collaboration in previous publications [16,17].

2 Experiment

The measurements were performed with the Large Acceptance Detector System (LADS) [18], which was built at the Paul Scherrer Institute (PSI) in Villigen, Switzerland to investigate multi-nucleon pion absorption (fig. 1). With the solid angle coverage of more than 98% of 4π and the low proton threshold of about 20 MeV, a large fraction of the phase space was accessible to LADS even at low incident pion energies.

The detector consisted of a plastic scintillator cylinder divided into 28 ΔE-E-E sectors, each 1.6 m in active length. The ends of the cylinder were closed by endcaps, each consisting of 14 ΔE-E plastic scintillator sectors. The scintillators stopped normally incident protons of up to 250 MeV. The trajectory information for charged particles was provided by two coaxial cylindrical multiwire proportional chambers (MWPCs) inside the plastic cylinder. Their angular resolution was about 1° FWHM. The target was a high-pressure gas cylinder of 25.7 cm length and 2 cm radius with carbon-fiber/epoxy walls of only 0.5 mm thickness to keep background and particle detection thresholds low.

The π^+ beam was defined by a set of plastic scintillation detectors that counted the individual pions and rejected particles in the beam halo. About 5% of the typical incident flux of about 3×10^6 momentum-analyzed pions per second was finally accepted by a 2 cm diameter scintillator placed about 50 cm upstream of the target center.

For the three target nuclei studied, N, Ar, and Xe, the target gas pressure was 40 bar, 28 bar, and 13 bar, respectively. The target temperature and pressure were monitored during the experiment and stayed constant within less than 1% throughout each specific target/beam run.

3 Data analysis

3.1 Data treatment

The data analysis was similar to that described in our earlier papers. Here only the most essential points will be stressed, and the reader is referred to ref. [16] for more details and figures showing the detector performance.

Events with track information (measured by the MWPCs) for at least two charged particles, and thus with a well-defined vertex, were analyzed. The spatial vertex resolution of less than 2.5 mm FWHM allowed a very efficient elimination of background events originating in the target walls. In order to estimate the remaining background from the target walls, data taken with an empty target

were analyzed in the same way as was the full target data. For the event sample selected with the vertex requirement the empty target background was small (*e.g.,* 0.3% at 239 MeV for the 3p final state). The requirement of at least two charged particles in the final state means that part of the absorption cross-section, with one or zero charged particles, has been missed in the present analysis.

To eliminate events near the edge of the detector acceptance, where the energy resolution drops, the polar angle of the data was limited to the range between 15 ° and 165 °. With this cut the solid angle covered was 96.6% of 4π.

Calibration constants obtained from ^{2}H and He data [19] were used to calibrate the gain and timing of each individual scintillator channel. For the charged particle separation into protons, pions and deuterons, conventional $E - \mathrm{d}E/\mathrm{d}x$ and E-TOF (time of flight) particle identification (PID) techniques were applied. The latter method was used for all charged particles with less than 10 MeV light deposited in the E-scintillators, because these were stopped in, or just passed through, the thin ΔE-counters.

The neutral particles were separated into neutrons and photons by a cut on the reduced TOF (defined as $1/\beta$). Particles below this cut (typically 1.5 ns) were identified as photons; those giving signals corresponding to more than 10 MeV were assumed to originate from neutral pions, while those which gave smaller signals were taken to be from nuclear de-excitation and ignored. Neutral signals with a reduced TOF above the cut were identified as neutrons, except that signals smaller than 5 MeV equivalent were taken to be noise and ignored. With this 5 MeV detection threshold, neutrons of more than 30 MeV kinetic energy were detected with about 35% efficiency and their kinetic energy was calculated from the TOF with a resolution of about 60% FWHM.

Pion absorption events were selected from other reaction channels by vetoing events with charged or neutral pions. Due to the photon detection efficiency (about 30%) some of the neutral pions were not detected and therefore such events remained in the absorption event sample; this will be discussed below. In the next step of the data analysis, each event was labelled according to the number of protons, deuterons and neutrons in the final state. In order to have a well-defined data sample a threshold of 30 MeV was introduced on the kinetic energy of each measured particle.

The final definition of an absorption event was thus: no detected pion (charged or neutral) and at least two charged particles (protons or deuterons) with kinetic energies above 30 MeV. For example the reaction channel labelled as 3p consisted of events with three energetic protons ($T_\mathrm{p} > 30$ MeV) and no detected neutron or deuteron above the 30 MeV threshold. Protons, neutrons or deuterons below this threshold were ignored in the analysis. Heavier particles such as tritium and alpha particles were not identified.

In these reactions, the recoil nucleus was in general produced in a highly excited state. Subsequently it could decay to its ground state with the emission of low-energy particles. The imposed 30 MeV threshold largely suppressed these "non-absorption" particles.

For each final channel two standard kinematic variables, the particle kinetic energy (T) and the polar angle (Θ), were histogrammed. In addition, two variables describing the global characteristics of an event were used, the missing energy and the missing momentum.

The missing energy is defined as

$$E_\mathrm{miss} = T_\pi + m_\pi - \sum_i T_\mathrm{p}^i + Q,$$

where T_π is the pion kinetic energy, m_π the pion mass, T_p^i the particle kinetic energy with the summation over all detected particles, and Q the reaction Q-value. In the case when all particles emitted in the reaction are detected, this quantity is almost equal to the excitation energy of the residual nucleus (the difference is the kinetic energy of the recoiling nucleus, which is small).

The missing momentum is defined as

$$\mathbf{P}_\mathrm{miss} = \mathbf{p}_\pi - \sum_i \mathbf{p}_\mathrm{p}^i,$$

where $\mathbf{p}_\pi$ is the pion momentum and $\mathbf{p}_\mathrm{p}^i$ are the momenta of all detected particles.

The number of observed absorption channels was large, up to 26 for the highest pion energy, and included particle multiplicities up to 6. As an example, the data for the 3p final state from the Ar target at pion beam energy 239 MeV are shown in fig. 2. The shaded areas are the experimentally observed distributions not corrected for any detection inefficiencies or acceptance. The lines show simulation results and will be discussed below. Note the large width of the missing energy spectrum of 250 MeV. Part of this width can be explained by undetected energetic particles, *e.g.* a 3p1n channel where the neutron escaped detection. The second contribution to the large missing energy is the excitation energy of the residual nucleus. Both effects will be discussed in more detail in sections 3.4 and 3.5.

3.2 Corrections

There are many effects which created detection inefficiencies and caused the observed channels to be non-pure. Some, like the neutron detection efficiency ($\approx$ 35%), particle reactions in the detector, solid angle and threshold acceptance, and MWPC efficiency were corrected for by Monte Carlo simulations. Others, like single charge exchange (SCX) contamination, charged pion mis-identification and proton-deuteron mis-identification, could not be corrected reliably with the Monte Carlo simulation and will be discussed here.

A charged pion could escape detection because of the less than full 4π solid angle coverage. It could also be mis-identified as a proton due to imperfect PID cuts. In the analysis of LADS data on light targets, where full kinematic reconstruction of the final state was possible, such events could be identified and removed. Here this was

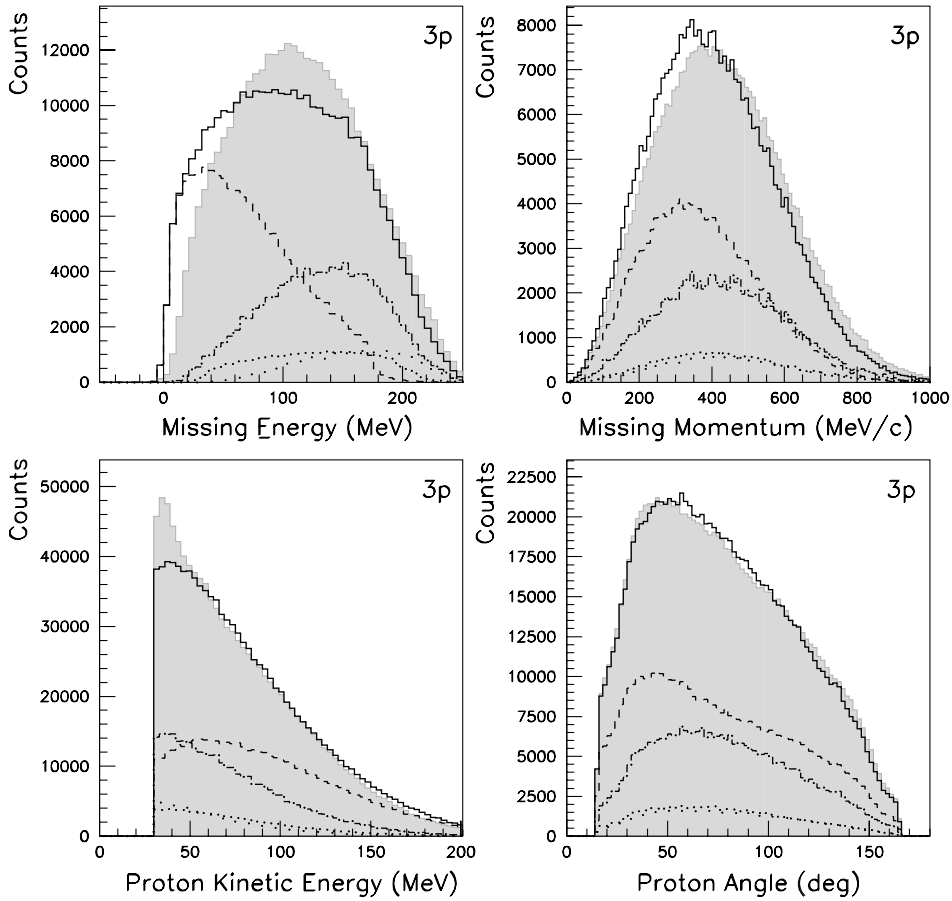

Fig. 2. Data from the Ar(π^+,3p) reaction at $T_\pi = 239$ MeV. The shaded areas are the experimental data. The solid lines show how these data are reproduced by the Monte Carlo simulations, with other lines representing individual Monte Carlo components: 3p (dashed), 3p1n (dashed-dotted), 4p (dotted) and 4p1n (wide dotted).

not possible and instead the magnitude of the correction obtained in a dedicated analysis of light targets [15] was used to estimate the contribution to the errors.

Similarly, due to imperfect PID cuts, some protons were classified as deuterons and *vice versa*. As in the previous case information about the size of this effect was available from an analysis of light targets [15]. This estimate was used as an additional contribution to the errors.

The situation is somewhat different with the π^0 background. Neutral pions decay into two energetic photons, with LADS detecting with some probability both, one, or none of the two. From the ratio of events with two and one photons detected the average photon detection efficiency could be found. This was determined to be $30 \pm 5\%$ and independent of the π^0 energy, which corresponds to roughly 50% π^0 detection efficiency. With the correction factor known the remaining π^0 contamination was subtracted from the absorption data. The subtracted cross-section depended on the final state, being larger for low multiplicity states, *e.g.*, 4.5% for 2p compared to 0.9% for 3p at 239 MeV. It also depended on the incident pion energy, *e.g.*, for the 3p final state the correction varied from 0.1% at 70 MeV to 3.9% at 330 MeV. The final errors have a component due to the π^0 subtraction (section 3.7).

3.3 Normalisation

The measured yields were normalised to the number of incident pions and target nuclei in order to determine the cross-sections. The procedure was the same as the one described in our earlier publications [16,19].

The number of target nuclei was determined from the target gas pressure and temperature. The areal densities varied from 4×10^{22} nuclei/cm^2 for N to 6×10^{21} nuclei/cm^2 for Xe. The estimated uncertainty on the number of scattering centers was 1%.

The number of incident pions was determined by the beam defining counters. To determine the number of pions which actually hit the target the counted pion rate was corrected for effects such as beam contamination with muons, pions lost through decay, pions lost through reactions in the scintillator and target, and pions missing the target. The largest correction came from the beam excluded by the target radial cut [16]. The amount of beam excluded by this cut varied from 30% at the lowest pion energy (70 MeV) to 8% for the highest energy (330 MeV). Other beam flux corrections were small, typically 1%–4%.

3.4 Monte Carlo simulations

Monte Carlo (MC) simulations were performed to correct the data for the acceptance and the detector inefficiencies and to assist in the interpretation of the data. In the simulations, the particles were tracked through a model of the detector using the GEANT software package. The experimental resolutions and hardware thresholds, as determined from the data for each scintillation counter and MWPC, were applied to the simulated events. The simulated data were then analyzed with the same set of programs as was used for the measured data. The effects of geometrical acceptance, energy thresholds and reaction losses in the detector, as well as inefficiencies of the wire chambers and the reconstruction code, were thus reflected in the simulated distributions in the same way as in those of the experimental data. The reliability of this procedure was tested earlier [19,20]. Twenty-six reaction channels were simulated, up to particle multiplicity six (*e.g.*, 5p1n), with about half of the channels containing one or more deuterons.

For each event generator a weight was included to represent the residual nucleus (spectator) momentum. This weighting factor was

$$\exp\left[-0.5\left(P_{\mathrm{res}}/\sqrt{3}\cdot P_{\mathrm{Fermi}}\right)^2\right],$$

where P_{res} is the residual nucleus momentum and P_{Fermi} reflects the width of the Fermi distribution. The value of P_{Fermi} was adjusted to 110 MeV/c to reproduce the average missing momentum. This value is similar to those used by Tacik *et al.* [21] and Bauer *et al.* [6].

The residual nucleus could be in an excited state, and so events were generated with an excitation energy distribution extending from 0 MeV to some maximum value. This maximum value was adjusted individually for each target and pion energy, as follows. Starting from a small value, about 50 MeV, it was incremented in steps of 30 MeV until the measured maximum of the missing energy distribution was reproduced (see fig. 2). No attempt (as in previous work [21]) was made to reproduce the exact shape of the missing energy, a flat excitation energy profile being used in all cases. The final maximum excitation energy used for the Ar target varied from 100 MeV for the lowest pion energy to 180 MeV for the highest. For the N target it was 80 MeV and for the Xe target 200 MeV. The accuracy of determining this parameter was about ±30 MeV and is taken into account in the error estimate.

The simplest event generator created final states with the final particles distributed uniformly over the phase space (PS), but weighted as described above. For the 2p channel a quasi-free absorption (QFA) event generator has been used in addition. In this model the pion was absorbed on a pn pair according to the deuteron cross-section [22]. For the 3p and 2p1n channels two additional event generators modelled simple two-step cascade processes: either an initial state interaction (ISI) followed by QFA, or QFA followed by a (hard) final-state interaction (FSI). For the ISI and FSI quasi-free πN and NN scattering processes were modelled and folded incoherently with the QFA process. Both of these models have been described in more detail in our previous paper [16].

The mixing fractions between the various event generators used for the 3p, 2p1n and 2p channels were adjusted by examining the observed kinetic energy and polar angle distributions. Unfortunately, there were no clear signatures in these distributions which allowed an unambiguous determination of the relative contribution of the different models. For the 2p1n channel the optimum PS/FSI ratio varied between 0.5/0.5 and 0.3/0.7 with the ISI contribution being always zero. For the 3p channel for the pion kinetic energies below 239 MeV the ISI contribution was set to zero and the PS/FSI ratio was roughly 0.5/0.5. For the two highest energies the PS contribution was replaced by ISI with the ISI/FSI ratio being between 0.5/0.5 and 0.3/0.7. For the 2p channel the PS/QFA ratio varied from 0.5/0.5 at low pion energies to 0.1/0.9 at high energies. As these ratios are very approximate, results obtained with pure PS models have also been determined. The final error estimate includes the difference between the two approaches.

It was not the primary purpose of this analysis to investigate signatures of possible reaction mechanisms, and the various types of event generators were used to improve the overall fit to the data and to assist the error analysis. Nevertheless, the discussion of the previous paragraph shows that, in the 3N final states, the fit quality was generally better if a significant amount of the FSI generator was included; this may be an indicator that such processes are important, which could be expected in these nuclei in view of the strength of the nucleon-nucleon cross-section. However, considering the lack of a clear kinematic signature, we do not draw quantitative conclusions.

3.5 Data fits

In order to determine the real final-state multiplicities, the simulated distributions were fitted simultaneously to the data with the normalisations of each distribution as free parameters. The resulting normalisations give a total yield for each observed final-state channel.

The fitting procedure to find the best set of MC normalisations was done in several steps. The maximum excitation energy of the residual nucleus was determined and the relative contributions of various MC models (ISI, FSI, QFA and PS) were adjusted (see section 3.4). The normalisations of the MC were then determined by requiring that the measured numbers of events in each channel were reproduced. These steps were iterated until satisfactory agreement with the shapes of the distributions was found.

The number of histograms used in this analysis was large (about 560) and the full set cannot be shown. Only a selected sample is presented in order to show the quality of the MC fits to the experimental data. Figures 3 and 4 show the kinetic energy and the polar angle of the protons from the observed 3p channel. The observed data are shown by the shaded area and the solid line shows the sum of all MC models contributing to this channel. Other lines show

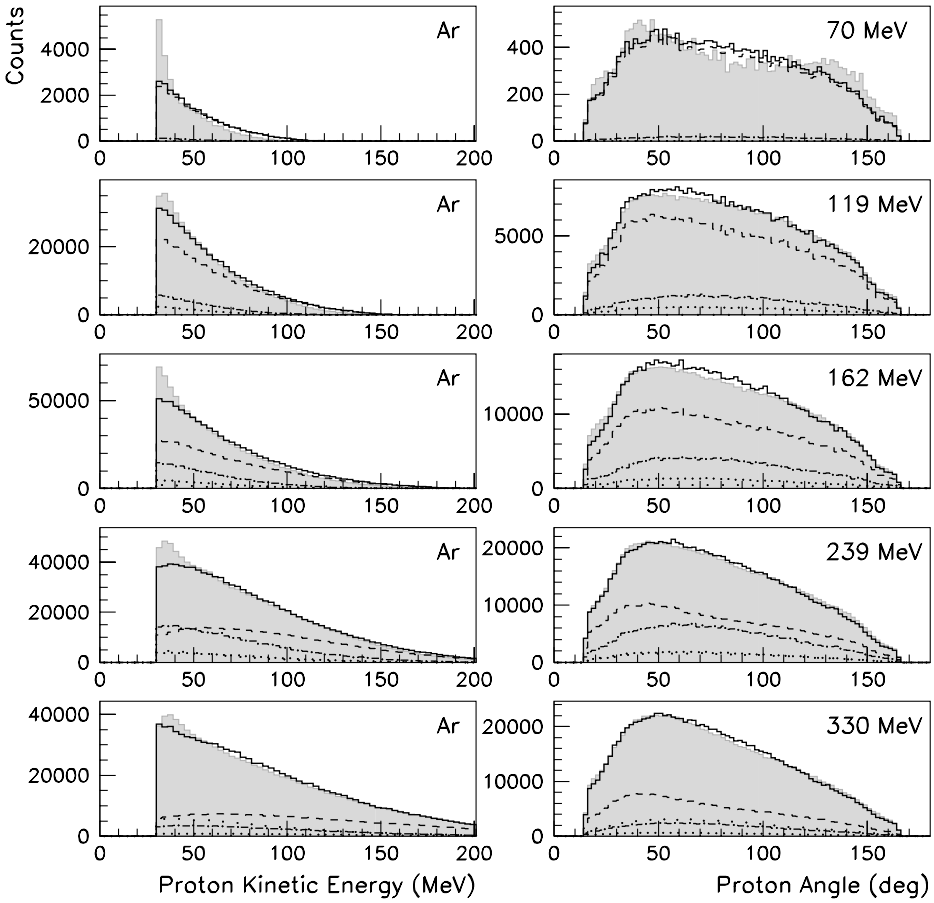

Fig. 3. Polar-angle and kinetic-energy distributions for the protons from the Ar(π^+, 3p) reaction at five pion energies. The shaded areas are the experimental data. The solid lines show how these data are reproduced by the Monte Carlo simulations. The meaning of the other lines is as in fig. 2.

individual contributions from a few dominant MC event generators. For the Ar target at the low pion energy the 3p event generator (dashed line) is by far the strongest contributor to the observed 3p channel (see fig. 3). With the increasing pion energy the contributions from the 3p1n (dashed-dotted) and 4p (dotted) event generators become more significant. In fig. 4 the three targets are compared at the same pion energy. There are no major differences between the three.

The overall fit quality is good. The largest discrepancy is for low proton kinetic energies ($T_\mathrm{p} < 50\,\mathrm{MeV}$) where there is always more experimental data than the MC predicts. This can be partly attributed to possible calibration problems of the thin (ΔE) plastic scintillators (discussed in more detail in our earlier paper [16]). One can also not exclude the possibility that the simple MC models used here do not explain the data in this region, *e.g.*, more FSI type of interactions would tend to increase the amount of protons at low energies.

Figures 5 and 6 compare the 3p reaction channel to a sample of results for other channels: 3p1n, 4p, 4p1n, 2p, 2p1n, 2p2n, 2p1d1n and 1p1d1n. In general, again the agreement of the data with the MC fits is very good for the polar-angle histograms, while for the kinetic-energy histograms the strength at low proton energies is always underestimated.

3.6 Reliability of the fitting procedure

Because of the detector's finite acceptance and efficiency, each observed final-state channel was populated by events with various real multiplicities. Similarly, simulated events from a given event generator, after being tracked through the model of the detector, populated a number of observed final state channels. To illustrate this, table 1 shows the contributions from various simulated distributions (with normalisations determined from fits to the data as described below) to the observed 3p channel, for Ar at 239 MeV. This shows that while the main contribution to the 3p channel is from 3p events, there are also significant contributions from other real multiplicities, *e.g.*, from 4p events with one proton sub-threshold, 3p1n events with the neutron undetected, etc. Similarly, table 2 shows how the simulated 3p events are distributed over various observed channels after being tracked through the detector.

With up to 26 observed channels this cross-feeding is very complex, but by simultaneously fitting the results

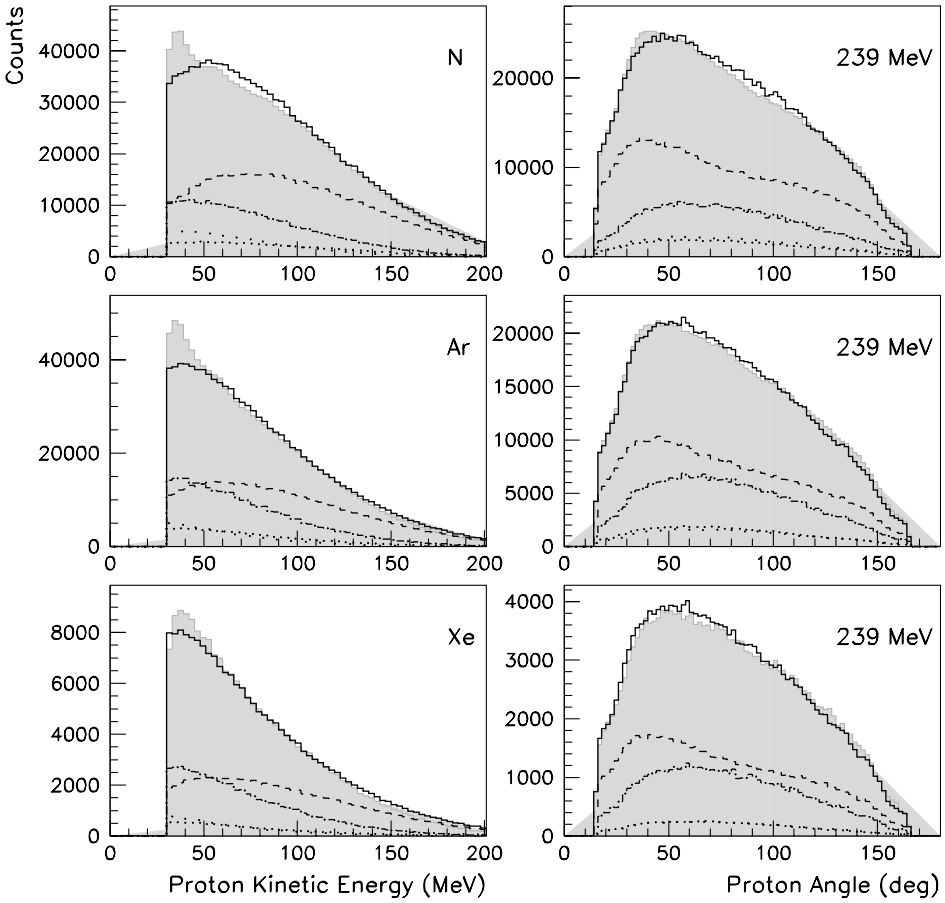

Fig. 4. Polar-angle and kinetic-energy distributions for the protons from the (π^+,3p) reaction on N, Ar and Xe targets at $T_\pi = 239$ MeV. The shaded areas are the experimental data. The solid lines show how these data are reproduced by the Monte Carlo simulations. The meaning of other lines is as in fig. 2.

Table 1. Contributions (in mb) from several Monte Carlo event generators to the observed Ar(π^+, 3p) channel at 239 MeV pion energy. Their sum is equal to the observed 3p cross-section.

MC event generators							
4p	4pn	3p	3pn	3p2n	3pdn	Other	Sum
1.7	1.5	9.2	5.9	0.3	0.4	0.9	19.9

Table 2. Distribution of events generated with the Ar(π^+, 3p) MC over the observed final channels at 239 MeV pion energy (in mb). The entry "1p + 0p" represents the unobserved cross-section with one or no proton in the final channel.

Observed final channels					
3p	2p	2pn	pd	"1p + 0p"	Sum
9.2	6.8	0.09	0.13	12.2	28.4

of all the simulations to the observed multiplicities and distributions, the real multiplicities can be deduced. Further, since the detector has a very large acceptance, there is generally little freedom to move strength between multiplicities while maintaining agreement between the results of the simulations and the data in all channels; this is less true for the neutron multiplicities, because of the relatively low detection efficiency, which will be discussed later.

The fitting procedure determined the strengths of the MCs required to fit the data. The strength of each MC then gives the acceptance and efficiency corrected cross-section for that channel, for 0 MeV particle threshold. For example, the 28.4 mb in table 2, representing the normalisation of the 3p in the fit to the data, is the Ar(π^+, 3p) partial cross-section.

A selection of partial cross-sections for Ar at 239 MeV pion energy is shown in table 3 for a few of the stronger final channels. The first column titled "Raw Data" shows the observed cross-sections as measured directly in the experiment. The last column labeled "Extrapolated to 0 MeV" shows the partial cross-sections corrected for all inefficiencies and for 0 MeV detection threshold. The second column labelled "30 MeV Threshold" shows cross-sections corrected for detector efficiencies and acceptances with a 30 MeV threshold, where all generated particles are required to have kinetic energies above 30 MeV. For the 3p model shown in table 2, out of the initial 28.4 mb

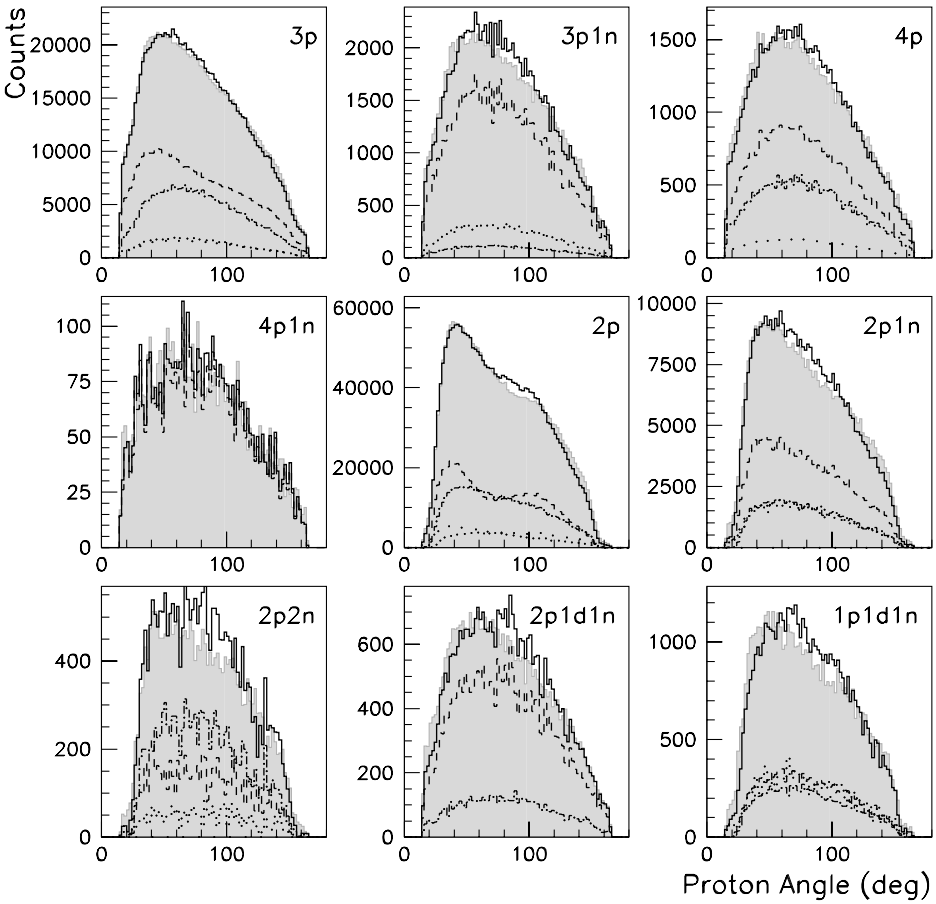

Fig. 5. Proton polar-angle distributions for selected channels following the π^++ Ar pion absorption reaction at $T_\pi = 239$ MeV. The shaded areas are the experimental data. The solid lines show how these data are reproduced by the Monte Carlo simulations. All other lines (dashed, dotted, wide-dotted and dashed-dotted) represent dominant components of the Monte Carlo fit.

3p cross-section only 60% (that is 17.1 mb) has 3 protons above the 30 MeV threshold. The rest is split into 9.3 mb 2p and 2 mb 1p contributions. Once a particle threshold is imposed other (non 3p) models start contributing to the 3p channel, *e.g.* 4p with one proton below 30 MeV. All these contributions have to be added together producing, in this case, a cross-section equal to 26.8 mb.

Some additional explanation may be helpful to understand the numbers in table 3. A naive expectation would be that with efficiency or acceptance correction a given partial cross-section should increase, but this is not necessarily true since some corrections are also subtracted. Consider the case where the 3p cross-section is corrected for the events lost due to a missed proton. These events appeared as 2p events and therefore are subtracted from the raw 2p cross-section. Sometimes such subtractions are larger than the additive corrections, resulting in the final cross-section being smaller. For example the 2p 30 MeV threshold cross-section is 72.9 mb but the cross-section extrapolated to 0 MeV is only 43.6 mb. This is because higher multiplicities are feeding the 2p channel strongly with the 30 MeV threshold; they are removed when particles with energies below 30 MeV are included.

Table 3. A selection of partial cross-sections (in mb) for the $\mathrm{Ar}(\pi^+, X)$ pion absorption reaction at 239 MeV pion energy. The column labeled "Raw Data" gives the directly measured yield. The column "30 MeV Threshold" gives the yield fully corrected for detector acceptance but with a 30 MeV kinetic energy threshold. The "Extrapolated to 0 MeV" column gives the yield extrapolated to 0 MeV threshold.

	Raw Data	30 MeV Threshold	Extrapolated to 0 MeV
5p	0.013 ± 0.001	0.04 ± 0.01	0.64 ± 0.13
4p	1.11 ± 0.10	2.0 ± 0.2	5.1 ± 1.0
3p	19.9 ± 1.2	26.8 ± 2.5	28.4 ± 4.0
3pn	2.0 ± 0.2	11.9 ± 1.3	33.2 ± 7.5
2p	69.8 ± 4.2	72.9 ± 5.8	43.6 ± 5.2
2p1n	11.9 ± 0.9	62.9 ± 6.6	$75. \pm 10.$
2p2n	0.67 ± 0.05	5.6 ± 1.0	$21. \pm 8.$
2pd	9.2 ± 1.0	10.3 ± 1.2	7.9 ± 1.4
pd	14.6 ± 2.3	9.8 ± 1.7	4.2 ± 1.0
pdn	3.0 ± 0.4	13.8 ± 2.4	10.6 ± 2.5

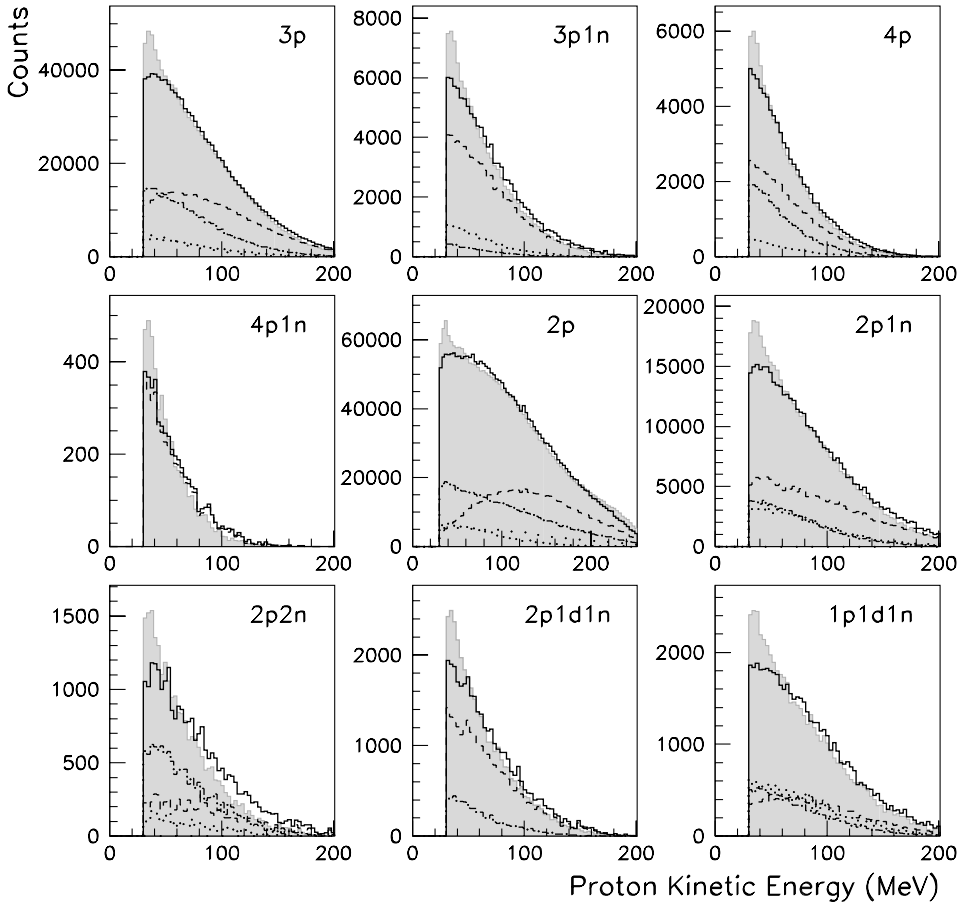

Fig. 6. Proton kinetic-energy distributions for selected channels following the π^++ Ar pion absorption reaction at $T_\pi = 239\,\mathrm{MeV}$. The shaded areas are the experimental data. The solid lines show how these data are reproduced by the Monte Carlo simulations. All other lines (dashed, dotted, wide-dotted and dashed-dotted) represent dominant components of the Monte Carlo fit.

3.7 Error analysis

In this section the errors on the partial cross-sections will be discussed. As an example individual error contributions to the Ar(π^+, 3p) reaction channel at five pion energies are shown in table 4. The statistical error is very small except for a few channels at high multiplicities. The fit errors, given by the fitting procedure (MINUIT), are also very small.

3.7.1 Normalisation

The error related to the beam normalisation varies with the pion beam energy, the dominating error coming from the beam-missing-target correction (see section 3.3). The pion flux upstream and downstream of the target was examined and the error taken to be half of the difference between the flux missing the target upstream and downstream (typically 5%–10%). The final normalisation errors were in the range 6%–10%, except at the lowest pion energy where it was 20%.

Table 4. Error contributions (in mb) to the Ar(π^+, 3p) pion absorption reaction cross-section. See text for the row label explanation.

	T_π (MeV)				
	70	118	162	239	330
Statistical	0.12	0.09	0.08	0.05	0.02
Normalisation	2.35	3.9	3.6	1.5	1.0
Fit	0.56	0.18	0.16	0.06	0.03
MC model	1.76	5.3	7.1	3.4	1.6
Excitation energy	1.88	4.6	6.2	1.1	1.8
SCX subtraction	0.11	0.35	0.47	0.28	0.15
Pion contamination	0.22	0.71	0.94	0.56	0.30
PID mis-identification	0.18	0.59	0.52	0.40	0.22
Final error	3.6	8.1	10.	4.0	2.6
Cross-section	11.8	35.3	47.	28.4	14.5

3.7.2 MC model and excitation energy

Because the analysis is model dependent there is an error associated with the choice of the MC models. Unfortu-

Table 5. Partial cross-sections (in mb) for the $Ar(\pi^+, X)$ pion absorption reaction. The results are acceptance corrected and for 0 MeV threshold.

T_π(MeV)	70	118	162	239	330
6p	–	–	–	–	0.13±0.04
5p	–	–	0.25±0.20	0.64±0.13	0.20±0.04
5pn	–	–	–	–	1.6±0.3
4p	–	2.1±1.0	4.9±1.2	5.1±1.0	3.2±0.6
4pn	–	–	3.9±1.3	7.4±1.8	3.7±1.0
4p2n	–	–	–	–	6.1±1.2
3p	11.8±3.6	35.3±8.1	47.±10.	28.4±4.0	14.5±2.6
3pn	≤1.7	13.2±3.2	31.8±8.0	33.2±7.5	16.0±3.9
3p2n	–	–	–	≤3.2	13.5±4.4
3p3n	–	–	–	–	5.4±2.3
2p	94.±23.	110.±28.	79.±16.	43.6±5.2	14.3±2.7
2p1n	40.±12.	91.0±21.	123.±23.	75.±10.	31.9±5.4
2p2n	–	–	≤10.	21.±8.	26.4±8.4
2p3n	–	–	–	≤1.0	9.1±2.1
3pdn	–	–	2.2 ±1.0	6.3 ±1.3	17.6±3.3
2p2d	–	≤2.	≤2.	2.4 ±0.5	3.9±1.0
3pd	–	2.4±1.0	3.8 ±1.0	5.5 ±1.1	1.8±1.0
p2dn	–	≤2.2	≤2.4	3.6 ±1.0	6.4±1.1
p2d	≤2.1	2.5±1.0	≤2.2	0.7 ±0.2	–
2pdn	≤1.1	8.3±2.2	12. ±3.2	19.±4.	24.8±4.4
2pd	5.5±1.9	15.±3.5	12. ±2.4	7.9 ±1.4	–
pd	18.±5.	18.±4.3	6.4 ±1.7	4.2 ±1.0	≤2.2
pdn	8.3±2.9	18.±5.0	16. ±4.	10.6±2.5	–
pd2n	–	–	–	6.0 ±1.5	20.3±4.5
2d	≤3.5	≤2.8	≤1.2	≤0.1	–
2dn	≤2.2	≤3.7	≤2.8	≤2.7	≤3.6
sum	180±43	320±65	351±40	283±28	225±17

nately, in general, there is no simple procedure to determine this uncertainty. For the three channels (3p, 2p1n and 2p) where more than one MC model was employed, a procedure similar to the one from our previous publications was used [16]. After the optimal ratio of the various MC models was established, the analysis was repeated using the PS models only. The error was estimated to be equal to the difference between the full (ISI, FSI, QFA) and the PS only results. For example the 3p partial cross-section at $T_\pi = 239$ MeV obtained with the PS model was equal to 25.0 mb (compared to 28.4 mb) which resulted in a 3.4 mb error. For other channels, where only the PS models were used, the model relative errors were set to be about equal to those of the three channels mentioned above.

The maximum excitation energy of the residual nucleus could only be determined with an accuracy of about ±20–30 MeV. To estimate the magnitude of the excitation-energy error, results were also obtained at the upper (+30 MeV) and lower (−30 MeV) limits. Half of the difference between the two sets of results was used as the error estimate.

3.7.3 π^0 subtraction and charged pion contamination

The single charge exchange subtraction has been discussed in more detail in section 3.2. The uncertainty associated with this correction is assumed to be equal to a quarter of its magnitude. This error depends on the pion beam momentum and the absorption final state. It varies between 7% (at high pion energy and low multiplicity final states, *e.g.*, 2p state at 330 MeV) and 1% (for most other cases).

Contamination of absorption events with events having a charged pion in the final state was estimated by MC. It was found that π2p events with an undetected pion contaminate 2p events at a level of 2%. Similarly π2p events with a pion mis-identified as a proton contaminate 3p events at a level of less than 1%. This is consistent with an evaluation done using pion absorption data on light targets [15] where the pion contamination was found to vary

Table 6. Partial cross-sections (in mb) for the pion absorption reaction on N, Ar and Xe targets at the pion beam energy of 239 MeV. The results are acceptance corrected and for 0 MeV threshold.

Target	N	Ar	Xe
5p	0.33 ± 0.05	0.64 ± 0.13	0.39 ± 0.14
4p	2.3 ± 0.4	5.1 ± 1.0	5.5 ± 1.3
4pn	4.0 ± 1.0	7.4 ± 1.8	9.8 ± 3.6
3p	15.6 ± 1.7	28.4 ± 4.0	37.4 ± 6.2
3pn	13.1 ± 2.3	33.2 ± 7.5	53 ± 14
3p2n	≤ 1.6	≤ 3.2	37 ± 14
2p	23.6 ± 3.0	43.6 ± 5.2	70 ± 21
2p1n	31.4 ± 6.1	$75. \pm 10.$	171 ± 34
2p2n	2.5 ± 1.2	$21. \pm 8.$	84 ± 53
2p3n	–	≤ 1.0	≤ 53
3pdn	4.8 ± 1.0	6.3 ± 1.3	10.0 ± 3.3
2p2d	1.7 ± 0.3	2.4 ± 0.5	3.0 ± 1.0
3pd	3.2 ± 0.4	5.5 ± 1.1	5.0 ± 1.1
p2dn	1.3 ± 1.0	$3.6 \pm 1.$	10.4 ± 2.6
p2d	–	0.7 ± 0.2	1.2 ± 0.2
2pdn	6.0 ± 1.0	$19. \pm 4.$	$46. \pm 12.$
2pd	4.1 ± 0.6	7.9 ± 1.4	11.0 ± 2.3
pd	1.2 ± 0.3	4.2 ± 1.0	15.0 ± 3.5
pdn	2.9 ± 1.0	10.6 ± 2.5	9.2 ± 3.4
pd2n	≤ 1.8	6.0 ± 1.5	66 ± 17
2dn	≤ 0.2	≤ 2.7	≤ 12
sum	$119. \pm 10.$	283 ± 28	676 ± 94

between 0.7% and 1.4%. An error of 2% was adopted as an upper limit for pion contamination in all final states.

3.7.4 Particle mis-identification

Due to imperfect PID cuts, some protons were classified as deuterons and *vice versa* (see section 3.2). MC simulations estimated the number of protons which appear as deuterons to be 1%–2% and 2%–3% for deuterons appearing as protons. This is consistent with the 2.7% found in the light target absorption data [15]. To be conservative a possible mixing factor of 3% is assumed here. This translates sometimes into much larger error estimates since the d/p ratio has to be included. For example for the 3pd channel (Ar at 239 MeV) 3% mixing from the 3p channel translates into an error of 6.5%. The corresponding error estimate for the 3p channel is only 1.4% since the number of 3p events is larger than 2p1d.

Due to the finite resolution the TOF cut to separate neutrons and photons may not be perfect, and some misidentification is expected especially for fast neutrons. By looking at the TOF histograms and extrapolating the photon peak beyond the cut an upper limit of 5% was found to be a conservative estimate for this error.

Reactions of charged particles in the scintillator material might result in incomplete detection of kinetic energy.

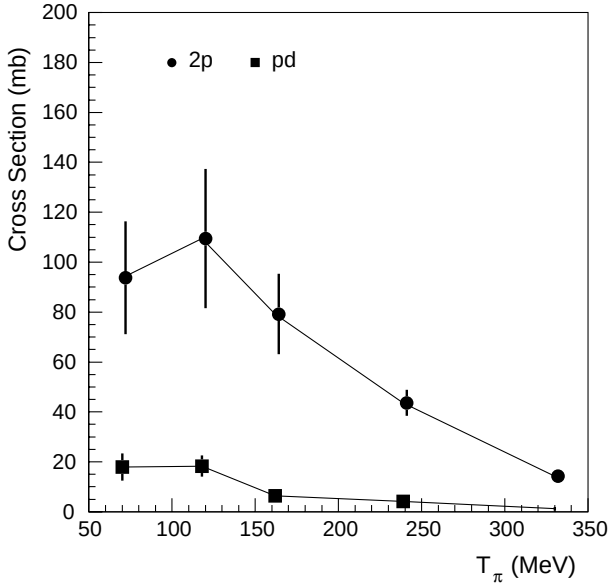

Fig. 7. The measured two-particle cross-sections (in mb) for the π^++ Ar pion absorption reaction as a function of pion kinetic energy. Cross-sections are corrected for all inefficiencies and extrapolated to 0 MeV threshold.

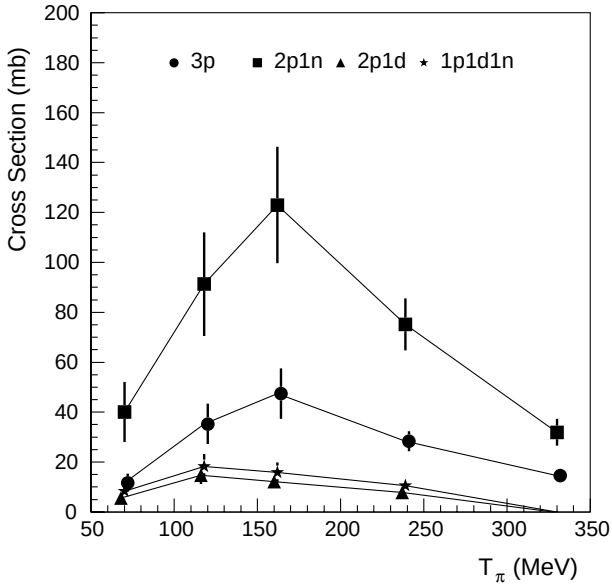

Fig. 8. The measured three-particle cross-sections (in mb) for the π^++ Ar pion absorption reaction as a function of pion kinetic energy. Cross-sections are corrected for all inefficiencies and extrapolated to 0 MeV threshold.

In extreme cases this might cause the particle to be ignored in the analysis. All reaction effects were corrected in the present work by Monte Carlo simulations, which means the results depend on the accuracy of the reaction cross-section tables included in the GEANT package. The agreement between the GEANT generated reaction correction was checked for the light target LADS data [20]. In the present analysis an error of 4% was included to account for reaction corrections.

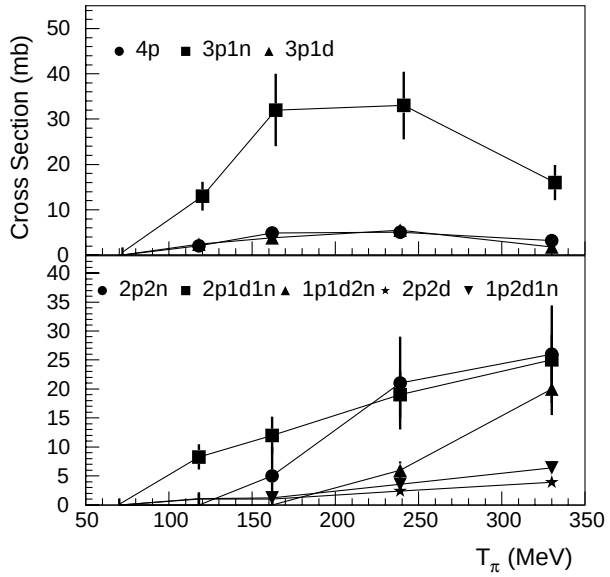

Fig. 9. The measured four-particle cross-sections (in mb) for the π^++ Ar pion absorption reaction as a function of pion kinetic energy. Cross-sections are corrected for all inefficiencies and extrapolated to 0 MeV threshold.

Channels with more than one neutron (2p2n, 2p3n and 3p2n) require special attention. The LADS neutron efficiency was about 35% which meant that for two neutrons and three neutrons the efficiency was 12% and 4%, respectively. Such low efficiency meant large correction factors and therefore large uncertainties. In addition the way neutrons interact with the detector can obscure the results. A neutron can re-scatter from one detector segment to another, simulating a two-neutron event (*e.g.*, a 2p1n event might look like a 2p2n). In principle such effects are included in the MC simulation but the accuracy depends critically on the neutron cross-sections defined in GEANT. This results in some correlation between the fitted cross-sections for the one, two and three neutron final states. The effect is relatively small for the cross-sections with one neutron in the final state. However, the two and three neutron states are weaker and the error due to the correlation can be up to 100% in some cases.

The error for the 2n/3n channels was determined in the following way: the number of raw counts was modified by introducing additional cuts (on the missing energy); the fits were rerun and the new set of partial cross-sections was established; the errors were taken as the difference between the standard and the modified sets of partial cross-sections. As an example consider the 2p2n channel for the Xe target at $T_\pi = 239$ MeV. The additional cut reduced the number of raw counts by only 8%, but the partial cross-section went down by almost 50%. The 2p2n cross-section decrease was compensated by an almost 100% increase in the 2p3n cross-section while the sum of 2p2n + 2p3n remained almost constant. Due to this uncertainty, in all neutron channels the minimum final error is 1 mb.

4 Results

4.1 Partial cross-sections

Final results are presented in tables 5 and 6. The partial cross-sections were corrected for all detection inefficiencies and were extrapolated to 0 MeV detection threshold as explained in the previous section. The errors were estimated according to the discussion presented in section 3.7 and include statistical, normalisation, SCX, pion contamination, PID mis-identification, excitation energy and model contributions added in quadrature. An empty entry in the tables means that the cross-section is below our detection limit and could not be determined. The detection limits are channel dependent and typically between 1 mb and 2 mb. The last row in each table is the sum of all partial cross-sections. We stress again that our channel definitions are exclusive, therefore "3p" means exactly three protons and no other energetic particle in the final state (except ignored low-energy photons and evaporation particles, or undetected heavy fragments).

Table 5 lists the partial cross-sections for pion absorption on the Ar target at five pion kinetic energies. table 6 lists the cross-sections for the N, Ar and Xe targets at 239 MeV pion energy. Note that the column for Ar at 239 MeV is shown twice in both tables for comparison.

Some deduced cross-sections have errors around 100%. These are usually weak channels where the main part of the error comes from model dependency and other Monte Carlo related sources (*e.g.*, neutron reaction correction). Such cross-sections are shown in tables 5 and 6 as upper limits (defined as the sum of the cross-section and the error).

4.2 Cross-sections for Ar as a function of pion energy

Selected Ar partial cross-sections from table 5 are plotted in fig. 7 to 9 as a function of pion kinetic energy. On each plot we select reaction channels having the same number of particles in the final state, with the deuteron taken as a single particle. In ^{4}He it was found [23] that deuteronic final states could be described as the result of final state pick-up reactions; *i.e.*, although two nucleons emerge as a deuteron, only one participated in the absorption process. We maintain this classification here.

Figure 7 shows that the 1p1d and 2p channels behave similarly, with the deuteronic final state becoming relatively stronger at lower energies, presumably reflecting the deuteron form factor's influence. This is seen again in fig. 8, with the deuteron yield also being broadly similar in shape. Figure 9, however, indicates a different behaviour for the deuteron channels: although the 3p1d channel follows the energy dependence of the 4p and 3p1n channels, the 2p1d1n channel continues to grow with pion energy, and even becomes relatively large, while the 1p1d2n, 1p2d1n and 2p2d channels only become significant at the highest two energies.

Figure 8 shows a preference for the 2p1n channel over the 3p channel, which also has been observed for absorption on ^{4}He [24] where the ratio of the 2p1n/3p yields

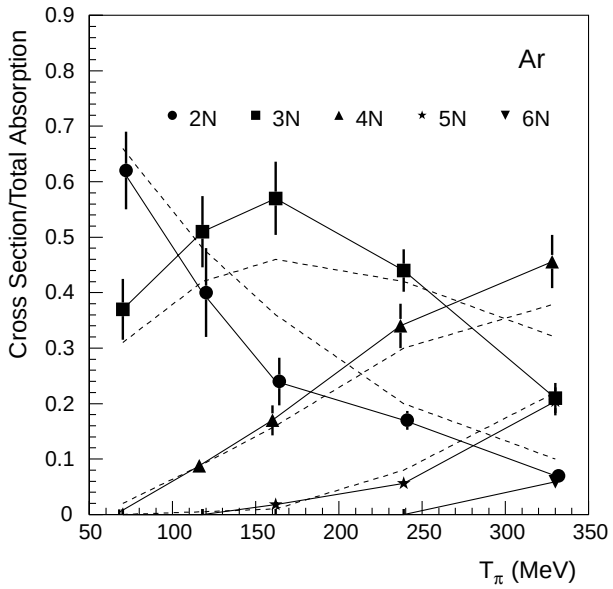

Fig. 10. Comparison of 2N (two particle), 3N, 4N, 5N and 6N cross-section fractions for the π^++ Ar pion absorption reaction as a function of pion kinetic energy. The plot shows cross-sections divided by the sum of all measured partial cross-sections. The solid lines connect the data points for a given multiplicity to guide the eye. The dashed lines are calculations with the simple phase space model of appendix A.

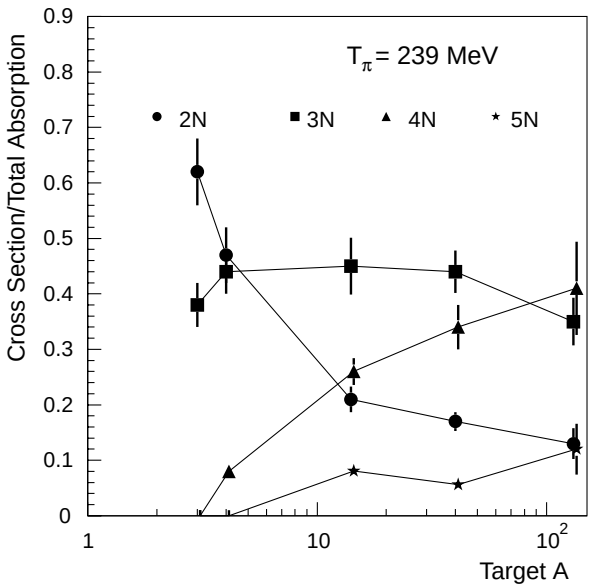

Fig. 11. Comparison of 2N (two particle), 3N, 4N and 5N partial cross-section fractions at $T_\pi = 239$ MeV as a function of target mass. The definition of the plotted quantities is the same as in fig. 10. The data for ^{3}He and ^{4}He are taken from references [20,24]. The solid lines connect the data points for a given multiplicity to guide the eye.

was around 2. This "preference" for neutrons over protons is also evident in fig. 9. However, the behaviour of the 2p2n channel is rather anomalous. Here it should be noted that the absolute cross-sections are small, as are the multi-neutron detection efficiencies, so that the total number of events is not large. As noted earlier there is no reliable way to distinguish between 4-body 2p2n and 5-body 2p3n states, so that it cannot be excluded that the rise in the 2p2n cross-section at higher pion energies is due to an undistinguished 2p3n contamination beyond the level of the assigned error.

Some simple conclusions can be drawn from looking at the three figs. 7–9. The energy at which the cross-sections peak moves from lower to higher values with the increase of the number of particles in the final state. Cross-sections for channels which include neutrons are typically larger than the ones with charged particles only. Deuteron channels typically have a strength between 10%–20% of a corresponding nucleonic channel.

4.3 Particle multiplicities

In order to present the final results in a more compact form we add the cross-sections corresponding to the same number of particles in the final state, again with deuterons counted as a single particle. The ratios of partial cross-sections divided by the sum of all partial cross-sections for the 2N-6N final states are plotted in fig. 10 for the Ar target at the five pion energies. One sees an increase of the particle multiplicity with pion energy. The 2N fraction of the absorption cross-sections, which dominates at the lowest energy, decreases in importance and becomes weak at the highest energy while the 3N fraction peaks around 160 MeV. Higher multiplicities gain strength with increasing pion energy.

The observed increase of the particle multiplicity with pion energy can be compared with an estimate from a simple phase space-based model, outlined in appendix A. This model contains four parameters, whose values are obtained by a simultaneous fit to all the data in fig. 10. The results are included in the figure, where it can be seen that the agreement is fairly good, especially in view of the strong energy dependence of the underlying πN and NN cross-sections.

The values of the parameters of the phase space model derived from the fit, 25 MeV for the mean binding energy, $(36+0.1\times T_\pi)$ MeV for the mean residual excitation energy and 9.8 fm for the scale parameter R, are all physically reasonable values. The parameter R determines the relative strength of the different multiplicities and the value determined can be related to an effective knock-out cross-section of the order of 100 mb, which is a reasonable scale for both πN and NN cross-sections. This suggests that the agreement between the data and the phase space model in fig. 10 is not accidental and that the final-state multiplicities are consistent with rescattering processes, with the yield being limited by the available phase space.

In fig. 11 similar ratios are plotted as a function of the target mass at one pion energy (239 MeV). To have a better overview data points for ^{3}He and ^{4}He from earlier LADS publications [20,24] have been included. A notable feature in this plot is that the fraction of the pion absorption cross-section going to the 3N final state hardly

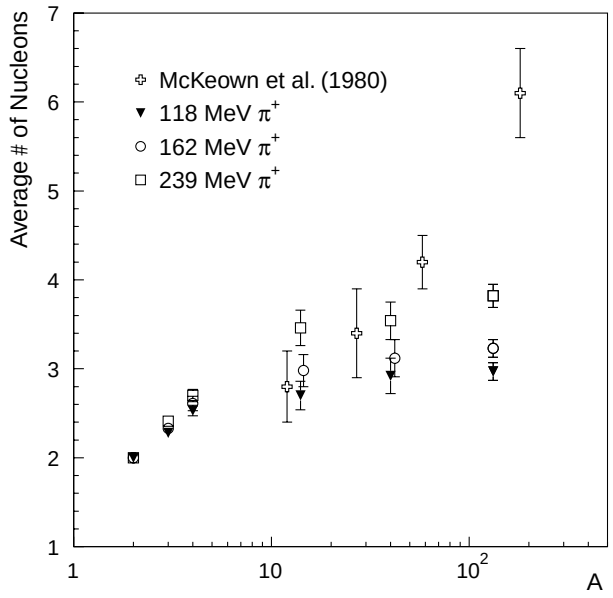

Fig. 12. Average final-state multiplicities as a function of target mass, compared to those of McKeown *et al.* [25], which are an average of three similar energies. The LADS points not obtained in this paper are taken from references [14,24,20].

changes over the whole mass range from ^{3}He to Xe. In addition, changes in 2N, 4N and 5N cross-section fractions between N and Xe are not large.

Figure 12 shows the average number of emitted energetic nucleons as a function of target mass and pion energy. The ^{3}He and ^{4}He data points are again taken from references [20,24]. The LADS average multiplicities are compared to earlier measurements by McKeown *et al.* [25]. Our data indicate a rather modest growth with A from ^{4}He to Xe, as already suggested by fig. 11. This weak A-dependence is consistent with the hypothesis just discussed, that the final-state multiplicities are largely determined by the available phase space. Note, however, that in a detailed study (ref. [16]) of the 3p channel the magnitude of the cross-section could not be explained by the simple ISI/FSI cascade models used in our simulations. These models are too crude to explain the kinematic distributions in detail or other, unknown, processes are present.

4.4 Summed cross-sections

The last rows in tables 5 and 6 present the sums of the partial cross-sections. The errors on these are smaller than those on the individual components, because the sum has much smaller fit, PID and model errors. In the partial cross-section these three errors are correlated, such that a range of different strengths for individual cross-sections is possible, but within an approximately constant sum. The summed cross-sections should be the total absorption cross-sections except that final states with less than two charged particles (protons or deuterons) have not been included.

Some of the data presented here have been previously analyzed with a method which was optimized for a total pion absorption determination and included the single charged-particle final states [15]. The absorption cross-sections found for the Ar target at the three pion energies 118 MeV, 162 MeV and 239 MeV were 393 ± 21 mb, 366 ± 22 mb and 282 ± 21 mb, respectively, and 107 ± 10 mb for the N target at 239 MeV. Except at the lowest-pion energy (118 MeV) these values agree very well with the summed partial cross-sections presented here. The summed cross-section at 118 MeV differs by 73 mb, which is close to the 65 mb estimated error of our measurement. However, it cannot be excluded that this difference reflects a significant contribution from single and zero charged channels at this energy as suggested by Gianneli *et al.* [13] using the model of Vincente-Vacas and Oset [26].

4.5 Comparison with previous measurements

The BGO-ball measurements at LAMPF [7,12,13] had a wide solid angle coverage and investigated absorption for a large range of targets (Li to Pb) and pion energies (50 MeV to 500 MeV). In their most recent publication, Giannelli *et al.* [13], pion absorption cross-sections at 120 MeV are presented for Al and Ni targets. Their inclusive 3p cross-section (3pxn) is 29/43 mb for the Al/Ni targets, respectively. A similar quantity derived from our data for Ar at 118 MeV is 49 ± 9 mb. For the inclusive 2p(2pxn) and 4p (4pxn) they find 172/230 mb and 1.0/2.0 mb. Our values for Ar are 301 ± 35 mb for the 2p and 2 ± 1 mb for the 4p channels. The level of agreement for all three inclusive cross-sections is reasonable considering the difference in the detector sensitivity and the analysis method. The exclusive 3p1n compares somewhat less well, our value of 13.2 mb being lower than the BGO-ball 20/33 mb. For the exclusive 2p1n channel the agreement is again good, our 91 mb compared to 92/124 mb.

The ^{16}O $(\pi^+, 3p)$ cross-section was measured by Bauer *et al.* at $T_\pi = 65$ MeV [6]. Through MC simulations the authors determined the 3N and 4N cross-sections. Their multi-nucleon (3N + 4N) fraction of the total absorption cross-section is equal to 34%. This is very close to the 37% given by our data for N at $T_\pi = 70$ MeV.

In a series of experiments the C$(\pi^+, 3p)$ reaction has been measured by Tacik *et al.* at $T_\pi = 130$ MeV–280 MeV [4,10,21]. In the most recent [10] of their papers these authors claim a surprising result that the 3p cross-section is very low and the 4N (defined as 3p1n and 4p) cross-section large. In contrast we find large cross-sections for 3p and 2p1n and a somewhat smaller 4N cross-section than in ref. [10]. We note that with the near full acceptance of LADS, the 3N and 4N cross-sections are constrained by the observed yields, while the co-planar acceptance of the CHAOS detector requires a more model dependent extraction of the partial cross-sections.

5 Summary

In the present paper the pion absorption reaction π^+ on Ar was studied at pion energies of 70, 118, 162, 239 and 330 MeV, and on N and Xe at 239 MeV. A total number of 26 absorption reaction channels with at least two energetic charged particles in the final state have been identified. The partial cross-sections split according to the number of protons, neutrons and deuterons in the final state have been determined.

Cross-sections for channels having the same number of particles peak at roughly the same pion kinetic energy, which rises with the increase in the number of particles in the final state. Cross-sections for channels which include neutrons are typically larger than the ones with charged particles only. Deuteron channels typically have the strength of between 10%–20% of a corresponding nucleonic channel. The data presented here demonstrate the importance of large acceptance, including for neutral particles, for the analysis of multi-particle final states.

The overall behaviour is rather smooth as a function of pion energy for all final states. The fractions of the pion absorption cross-section going to final states with 2, 3, 4 and 5 particles reach saturation values already for nitrogen, and within errors, stay the same for N, Ar and Xe targets. Comparison to a simple phase-space model suggests that the final state multiplicities for all these nuclei are substantially determined by the available phase space.

We thank the staff of the Paul Scherrer Institute for the technical support provided to this experiment. This work was supported in part by the German Bundesministerium für Forschung und Technologie, the German Internationales Büro der Kernforschungsanlage Jülich, the Swiss National Science Foundation, the U.S. Department of Energy, and the U.S. National Science Foundation.

Appendix A. A phase space estimate of particle multiplicities

The cross-section of the pion absorption for the final state with n particles can be represented in the form

$$\sigma_n(T_\pi) = \frac{(2\pi)^4}{4M_A p_\pi} \int \left|\mathcal{M}_{n+X}(T_\pi)\right|^2 \mathrm{d}\Phi_n \, \mathrm{d}\Phi_X, \qquad (A.1)$$

where $\mathcal{M}_{n+X}(T_\pi)$ is the pion absorption amplitude for the final state with n "energetic" particles and some spectators X, $\mathrm{d}\Phi_n$ and $\mathrm{d}\Phi_X$ are the corresponding phase spaces, M_A is the target mass, and p_π is the pion momentum in the lab system. As long as we are interested only in the multiplicities of the energetic particles, we can introduce the effective average amplitudes squared:

$$\sigma_n(T_\pi) = \frac{(2\pi)^4}{4M_A p_\pi} \overline{|\mathcal{M}_n(T_\pi)|^2}\, \tilde{\Phi}_n, \qquad (A.2)$$

where $\tilde{\Phi}_n$ is the phase space available to the energetic particles, which is effectively reduced due to the excitation of the spectators.

The phase space model involves two assumptions. First, the ratio of the matrix elements corresponding to the final states with n and $(n+1)$ particles does not depend on n and the initial pion energy:

$$\frac{\overline{|\mathcal{M}_{n+1}(T_\pi)|^2}}{\overline{|\mathcal{M}_n(T_\pi)|^2}} = R^2, \qquad (A.3)$$

where R is some parameter of dimension of length. Second, the effective n-particle phase space is given by

$$\tilde{\Phi}_n = \int \delta\Big(m_\pi + T_\pi - \sum_{i=1}^{n}(E_n - m) - \Delta(T_\pi, n)\Big) \times \delta\Big(\sum_{i=1}^{n} \mathbf{k}_i\Big) \prod_{i=1}^{n} \frac{\mathrm{d}^3\mathbf{k}_i}{(2\pi)^3 2E_i}. \qquad (A.4)$$

Here $E_i = \sqrt{m^2 + \mathbf{k}_i^2}$ is the energy of the nucleon with the momentum $\mathbf{k}_i$ in the final state and $\Delta(T_\pi, n)$ is the kinetic energy carried away by the spectators, for which we use the following parametrization:

$$\Delta(T_\pi, n) = nB + E_X + \zeta T_\pi, \qquad (A.5)$$

where B is the effective nucleon binding energy, and the excitation energy of the spectators $(E_X + \zeta T_\pi)$ is assumed to be a linear function of the pion energy.

Using this simple model one can reproduce the main features of the energy dependence of the branching ratios for the Ar target. The result is shown in fig. 10 for $R = 9.8$ fm, $B = 25$ MeV, $E_X = 36$ MeV, $\zeta = 0.1$; the parameters have been determined from the fit of two branching ratios $BR_{2,3}(T_\pi) = BR_2(T_\pi) + BR_3(T_\pi)$ and $BR_{4,5}(T_\pi) = BR_4(T_\pi) + BR_5(T_\pi)$. It would be naive to expect better agreement, especially because the energy dependence of the amplitudes is quite strong in the case concerned.

The value of R deserves a short comment. It can be easily shown in a cascade-like model that the characteristic scale of the ratio defined by eq. (A.3) has the form

$$R^2 \sim (2\pi)^3 |f|^2 \frac{m}{k^2 r}, \qquad (A.6)$$

where f is the amplitude of the knock-out of an additional nucleon, m is the nucleon mass, k is the characteristic momentum of the particle in the intermediate state, r is the average distance between the nucleons in the target, and the relation $kr > 1$ is assumed.

With $R \approx 10$ fm this corresponds to an effective knock-out cross-section $\sigma = 4\pi|f|^2$ of the order of 10^2 mb; that is in the range of physically meaningful values, both for the elastic πN scattering (ISI) and the elastic NN scattering (FSI). This allows us to conclude that the fair agreement between the data and the phase space model in fig. 10 indicates that the ratio of the amplitudes for the different multiplicities, eq. (A.3), is determined by the strength of the rescattering mechanisms. In the energy range of the present experiment, the gross feature of the energy dependence of the yields of different multiplicities is determined mainly by the available phase space.

References

1. A. Altman et al., Phys. Rev. C **34**, 1757 (1986).
2. W.J. Burger et al., Phys. Rev. C **41**, 2215 (1990).
3. D.J. Mack et al., Phys. Rev. C **45**, 1767 (1992).
4. R. Tacik et al., Phys. Rev. C **32**, 1335 (1985).
5. W. Brückner et al., Nucl. Phys. A **469**, 617 (1987).
6. Th.S. Bauer et al., Phys. Rev. C **46**, R20 (1992).
7. R.D. Ransome et al., Phys. Rev. C **45**, R509 (1992).
8. H.J. Weyer, Phys. Rep. **195**, 295 (1990).
9. C.H.Q. Ingram, Nucl. Phys. A **553**, 573c (1993).
10. R. Tacik et al., Phys. Rev. C **57**, 1295 (1998).
11. G.M. Huber et al., Nucl. Phys. A **624**, 623 (1997).
12. M.K. Jones et al., Phys. Rev. C **48**, 2800 (1993).
13. R.A. Giannelli et al., Phys. Rev. C **61**, 054615 (2000).
14. N.K. Gregory, Ph.D. thesis, MIT, 1999.
15. D.C. Rowntree et al., Phys. Rev. C **60**, 054610 (1999); D.C. Rowntree, Ph.D. thesis, MIT, 1995.
16. B. Kotliński et al., Eur. Phys. J. A **1**, 435 (1998).
17. D. Androić et al., Phys. Rev. C **53**, R2591 (1996).
18. T. Alteholz et al., Nucl. Instrum. Methods A **373**, 374 (1996).
19. A. Lehmann et al., Phys. Rev. C **55**, 2931 (1997).
20. A.O. Mateos et al., Phys. Rev. C **58**, 942 (1998); A.O. Mateos, Ph.D. thesis, MIT, 1995.
21. R. Tacik et al., Phys. Rev. C **40**, 256 (1989).
22. B.G. Ritchie, Phys. Rev. C **44**, 533 (1991).
23. M. Planinić et al., Phys. Rev. C **61**, 054604 (2000).
24. A. Lehmann et al., Phys. Rev. C **56**, 1872 (1997).
25. R. McKeown et al., Phys. Rev. Lett. **44**, 1033 (1980).
26. M. Vincente Vacas, E. Oset, Nucl. Phys. A **568**, 855 (1994).